Radiation Damage Effects

Ren-Yuan Zhu

Contents

Abstract

Radiation damage is an important issue for particle detectors operated in a hostile environment where radiations from ionization dose, protons, and neutrons are expected. This is particularly important for future high energy physics detectors designed for the energy and intensity frontiers. This chapter describes the radia-

R.-Y. Zhu (✉)
High Energy Physics Group, Physics, Mathematics and Astronomy Division, California Institute of Technology, Pasadena, CA, USA
e-mail: zhu@hep.caltech.edu

tion damage effects in inorganic scintillators, including scintillation mechanism damage, radiation-induced phosphorescence, radiation-induced absorption, and radiation-induced light output degradation. While radiation damage in halides is attributed to the oxygen/hydroxyl contamination, it is the structure defects, such as the oxygen vacancies, which cause damage in oxides. Various material analysis methods used in investigations of the radiation damage effects as well as the improvement of crystal quality through systematic R&D are also discussed.

Introduction

Total absorption shower counters made of inorganic crystal scintillators have been known for decades for their superb energy resolutions and detection efficiencies (Gratta et al. 1994) (▶ Scintillators and Scintillation Detectors , ▶ Calorimeters). In high energy and nuclear physics experiments, large arrays of scintillating crystals of up to more than ten cubic meters have been assembled for precision measurements of photons and electrons. These crystals are working in a radiation environment, where various particles, such as γ-rays, charged hadrons, and neutrons, are expected. Table 1 (Mao et al. 2008) lists basic properties of heavy crystal scintillators commonly used in high energy physics (HEP) detectors. They are thallium-doped sodium iodide (NaI(Tl) or NaI:Tl), thallium-doped cesium iodide (CsI(Tl) or CsI:Tl), undoped CsI, barium fluoride (BaF_2), bismuth germanate ($Bi_4Ge_3O_{12}$ or BGO), lead tungstate ($PbWO_4$ or PWO), and cerium-doped lutetium oxyorthosilicate ($Lu_2(SiO_4)O$:Ce or LSO) (Melcher and Schweitzer 1992) and cerium-doped lutetium yttrium oxyorthosilicate ($Lu_{2(1-x)}Y_{2x}SiO_5$:Ce, LYSO) (Cooke et al. 2000; Kimble et al. 2002). All crystals have either been used in, or actively pursued for, high energy and nuclear physics experiments. Some of them, such as NaI:Tl, CsI:Tl, BGO, LSO, and LYSO are also widely used in the medical industry.

All known crystal scintillators suffer from radiation damage (Zhu 1998). There are three possible radiation damage effects in crystal scintillators: (1) scintillation mechanism damage, (2) radiation-induced phosphorescence (afterglow), and (3) radiation-induced absorption (color centers). A damaged scintillation mechanism would reduce crystal's scintillation light yield and cause a degradation of crystal's light output. It may also change crystal's light response uniformity for large size crystals used to construct total absorption calorimeters since radiation dose profile is usually not uniform along the crystal length. Radiation-induced phosphorescence, commonly called afterglow, causes an increased dark current in photo-detectors, and thus an increased readout noise. Radiation-induced absorption reduces crystal's light attenuation length (Ma and Zhu 1993a), and thus crystal's light output and possibly also crystal's light response uniformity.

Table 2 summarizes radiation damage effect for various crystal scintillators. There is no experimental data supporting scintillation mechanism damage. All crystal scintillators studies so far, however, suffer from radiation-induced phosphorescence and radiation-induced absorption.

Table 1 Properties of heavy crystal scintillators

Crystal	NaI:Tl	CsI:Tl	CsI	BaF$_2$	BGO	PWO	LSO/LYSO
Density(g/cm^2)	3.67	4.51	4.51	4.89	7.13	8.3	7.40
Melting point (°C)	651	621	621	1280	1050	1123	2050
Radiation length (cm)	2.59	1.86	1.86	2.03	1.12	0.89	1.14
Moliere radius (cm)	4.13	3.57	3.57	3.10	2.23	2.00	2.07
Interaction length (cm)	42.9	39.3	39.3	30.7	22.7	20.7	20.9
Refractive index[a]	1.85	1.79	1.95	1.50	2.15	2.20	1.82
Hygroscopicity	Yes	Slight	Slight	No	No	No	No
Luminescence[b] (nm) (at Peak)	410	560	420 310	300 220	480	425 420	420
Decay time[b] (ns)	245	1220	30 6	650 0.9	300	30 10	40
Light yield[b,c]	100	165	3.6 1.1	36 4.1	21	0.30 0.077	85
d(LY)/dT[b,d] (%/°C)	−0.2	0.4	−1.4	−1.9 0.1	−0.9	−2.5	−0.2
Experiment	Crystal Bball	CLEO *BaBar* BELLE BES III	KTeV Mu2e-I	TAPS Mu2e-II	L3 BELLE	CMS ALICE PrimEx Panda	COMET HERD CMS

[a] At the wavelength of the emission maximum
[b] Top line: slow component, bottom line: fast component
[c] Relative light yield of samples of 1.5 X_0 and with the PMT QE taken out
[d] At room temperature

Table 2 Radiation damage in crystal scintillators

Item	CsI:Tl	CsI	BaF$_2$	BGO	PWO	LSO/LYSO
Scintillation mechanism	No	No	No	No	No	No
Phosphorescence (afterglow)	Yes	Yes	Yes	Yes	Yes	Yes
Absorption (color centers)	Yes	Yes	Yes	Yes	Yes	Yes
Recover at room temperature	Slow	Slow	No	Yes	Yes	No
Dose rate dependence	No	No	No	Yes	Yes	No
Thermally annealing	No	No	Yes	Yes	Yes	Yes
Optical bleaching	No	No	Yes	Yes	Yes	Yes

Radiation-induced absorption is caused by a process called color center formation, which may recover spontaneously under the application temperature through a process called color center annihilation. If so, the damage would be dose rate dependent (Ma and Zhu 1993b; Zhu 1997). If radiation-induced absorption does not recover, or the recovery speed is very slow, however, the color center density would increase continuously under irradiations until all defect traps are fully filled. In this

case the corresponding radiation damage effect does not depend on the dose rate applied.

Color centers may also be annihilated thermally by heating the crystal to a high temperature through a process called thermal annealing, or optically by injecting light of various wavelength through a process called optical bleaching (Ma and Zhu 1993b). The recovery process, either spontaneous or applied through thermal annealing or optical bleaching, reduces the color center density, or the radiation-induced absorption. The recovery process, however, also introduces an instability in crystal's transparency, so is crystal's light output. In this case, a precision monitoring system is mandatory to follow variations of crystal's transparency, and provide corrections for crystal's light output calibration.

Radiation damage caused by charged hadrons and neutrons may differ from that caused by ionization dose or γ-rays. Studies (Huhtinen et al. 2005) on proton-induced radiation damages in PWO crystals, for example, show a very slow (or no) recovery under room temperature, which seems contrary to the radiation damage caused by γ-rays. This leads to a cumulative proton-induced damage in PWO with no dose rate dependence.

Radiation damage level may also be different at different temperature for crystals with dose rate dependent damage since the spontaneous recovery speed is temperature dependent. PWO crystals used at low temperature, for example, suffer more damage than that at high temperature (Semenov et al. 2007).

Commercially available mass produced crystals may not meet the quality required for high energy physics detectors. The quality of mass produced crystals thus need to be improved by removing harmful impurities and/or defects in the crystal. The rest of this chapter discusses radiation-induced damage phenomena in inorganic scintillators, the origin of the radiation damage in halides and oxides as well as the improvement of the quality of commercially available crystals.

All data presented in this chapter, except that specified, are measured for full size crystals adequate for total absorption calorimeters, which are typically 18 to 25 X_0 long. Since both the radiation-induced phosphorescence and absorption are of the bulk effect, it is important that full size crystals are used in radiation damage studies.

Scintillation Mechanism Damage

Experimental data show that crystal's scintillation mechanism is not damaged by radiation. This is observed for irradiations of γ-rays, neutrons as well as charged hadrons (Huhtinen et al. 2005; Batarin et al. 2003). A common approach is to compare the shape of the emission spectra measured before and after irradiations. It is well known that the measured intensity of emission suffers from a large systematic uncertainty caused by sample position and orientation, sample surface quality, and internal absorption. Care thus should be taken in such measurements to maintain a well-controlled location of the sample and excitation source, and avoid emission light going through crystal bulk so that the measured emission spectrum is not affected by the radiation-induced absorption.
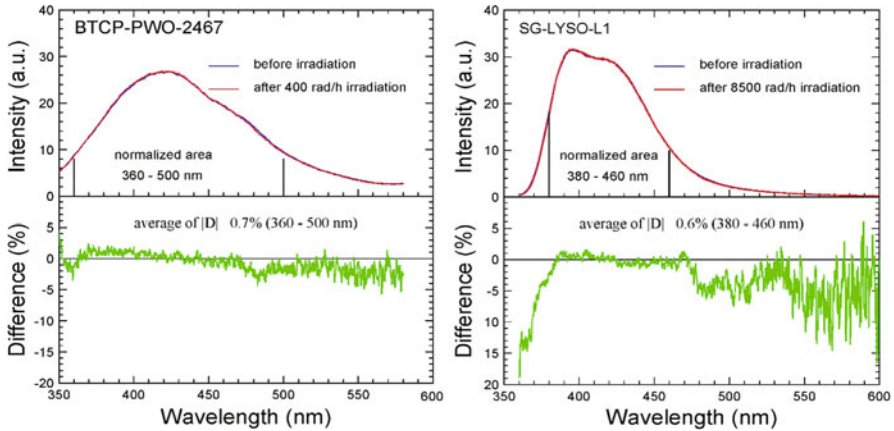
Fig. 1 Normalized photo-luminescence spectra measured before (blue) and after (red) γ-ray irradiation and corresponding difference (green) are shown as a function of wavelength for a PWO sample (left) and an LYSO sample (right)

The top plots of Fig. 1 show the photo-luminescence spectra measured before (blue) and after (red) γ-ray irradiations for a PWO sample (left) and an LYSO sample (right). These spectra are normalized to an integration around the emission peaks as shown in the figures. The relative difference between these normalized spectra (green) is shown in the bottom. Also shown in the bottom plots are the average of the absolute values of the relative difference, which are 0.7% and 0.6%, respectively, for PWO and LYSO. Such differences are much lower than the 1% systematic uncertainty of the measurements, showing that no statistically significant difference is observed between the photo-luminescence spectra taken before and after irradiations for both PWO and LYSO, indicating no damage to the scintillation mechanism. Similar investigations show that there is no scintillation mechanism damage observed for BGO (Zhu et al. 1991), BaF$_2$ (Zhu 1994), and CsI:Tl (Zhu et al. 1996a) as well. This conclusion is also supported by more complicated measurements of the light response uniformity before and after irradiations with a nonuniform dose profile (Batarin et al. 2003).

Radiation-Induced Phosphorescence and Energy Equivalent Readout Noise

Radiation-induced phosphorescence is observed by measuring photo-current during and after radiation is turned off. The left plot of Fig. 2 shows the γ-ray-induced photo-current after radiation, normalized to that during the irradiation, as a function of time during and after γ-ray irradiations for several crystal samples: PWO, BGO, and LSO/LYSO. All samples are of full size adequate for calorimeter applications. The amplitude of the normalized phosphorescence is at a level of 10^{-5} for BGO
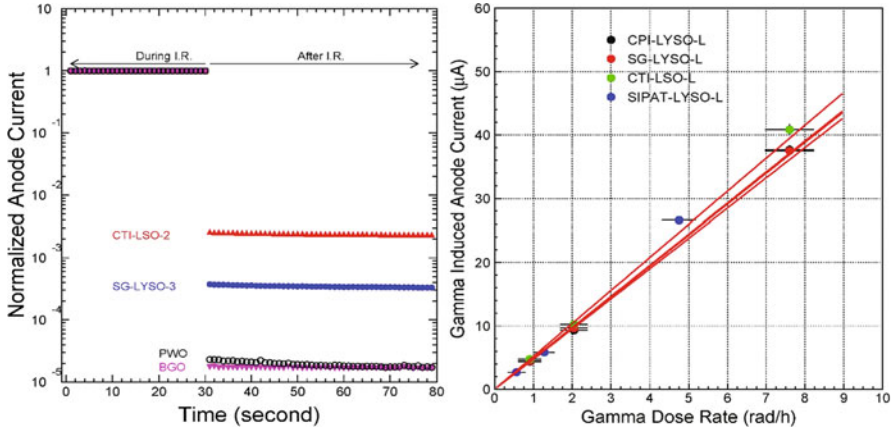
Fig. 2 Left: Normalized anode current is shown as a function of time during and after γ-ray irradiations for BGO, PWO, LSO, and LYSO samples. Right: γ-ray-induced anode photo-current is shown as a function of the dose rate applied to LSO and LYSO samples

and PWO, 3×10^{-4} for LYSO, and 2×10^{-3} for LSO, showing that LYSO has a smaller phosphorescence, or afterglow, than LSO.

The right plot of Fig. 2 shows γ-ray-induced anode photo-currents as a function of the γ-ray dose rate applied to several LSO and LYSO samples. Consistent slopes are observed for all samples because of the similar light yield of these samples. These slopes may be used to extract the readout noise in electron numbers for the crystal and photo-detector combination in a particular integration gate, which can then be converted to the energy equivalent readout noise by normalizing to the crystal's light output (Mao et al. 2009a, b). Because of its high light yield (200 times PWO and 5 times BGO) and short decay time (40 ns), the energy equivalent readout noise in LSO and LYSO is an order of magnitude lower than that in PWO for both γ-ray and neutron irradiations.

Radiation-Induced Absorption

The main consequence of radiation damage in scintillation crystals is radiation-induced absorption, or color center formation. Depending on the type of the defects in the crystals, color centers may be electrons located in anion vacancies (F center), holes located in cation vacancies (V center), and interstitial anion atoms (H center) or ions (I center), etc. Radiation-induced absorption is measured by comparing the longitudinal optical transmittance spectra measured after and before irradiation. A spectrophotometer of good quality provides systematic uncertainties as low as 0.2%.

Figure 3 shows longitudinal transmittance spectra as a function of wavelength measured before and after several steps of irradiations for halide crystals: CsI(Tl)
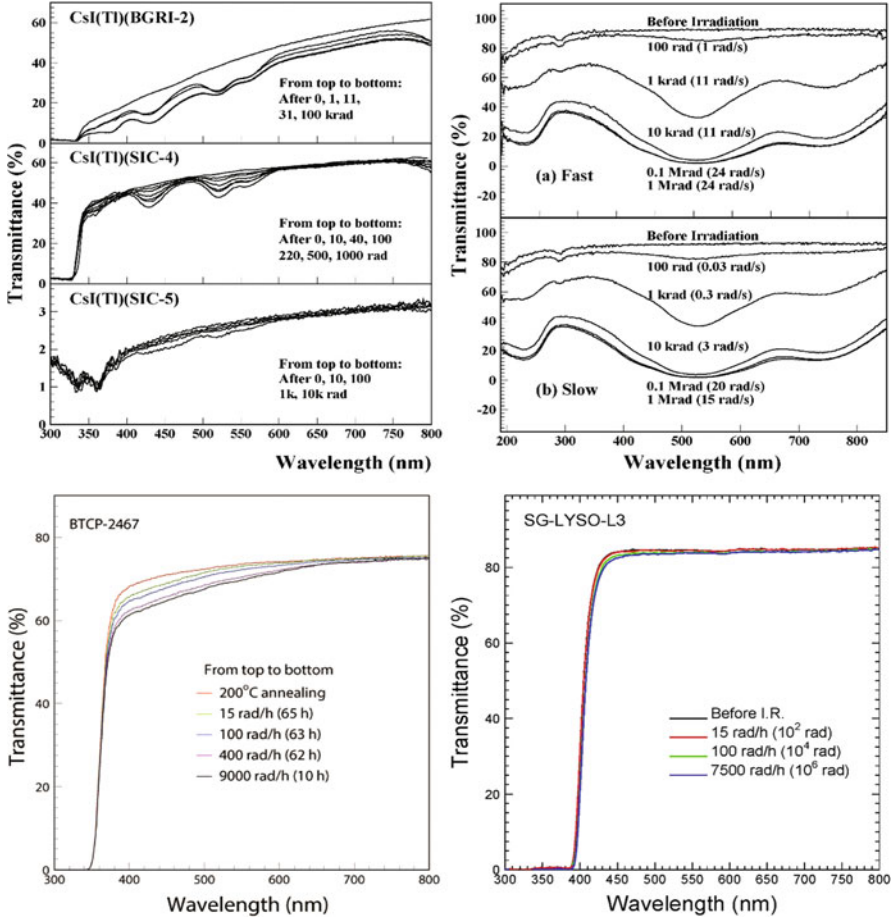
Fig. 3 The longitudinal transmittance spectra measured before and after several steps of the irradiation are shown as a function of wavelength for several CsI(Tl) (top left), a BaF$_2$ (top right), a PWO (bottom left), and an LYSO (bottom right) crystal samples

(top left) and BaF$_2$ (top right), and oxide crystals: PWO (bottom left) and LYSO (bottom right). While the color center width appears narrow in CsI(Tl), it is relatively wide in other crystals. It is interesting to note that the CsI(Tl) sample SIC-5 suffers much less radiation damage than other two CsI(Tl) samples since it was grown with a scavenger in the melt to remove the oxygen contamination, which is an effective approach to improve radiation hardness for halide crystals as discussed later in section "Damage Mechanism in Alkali Halide Crystals and CsI:Tl Development." For the BaF$_2$ sample we also notice that the damage levels of the longitudinal transmittance spectra are identical for the same integrated dose, while the fast dose rate (top) is up to a factor of 30 of the slow rate (bottom). Such a dose rate independence is expected since no recovery at the room temperature was
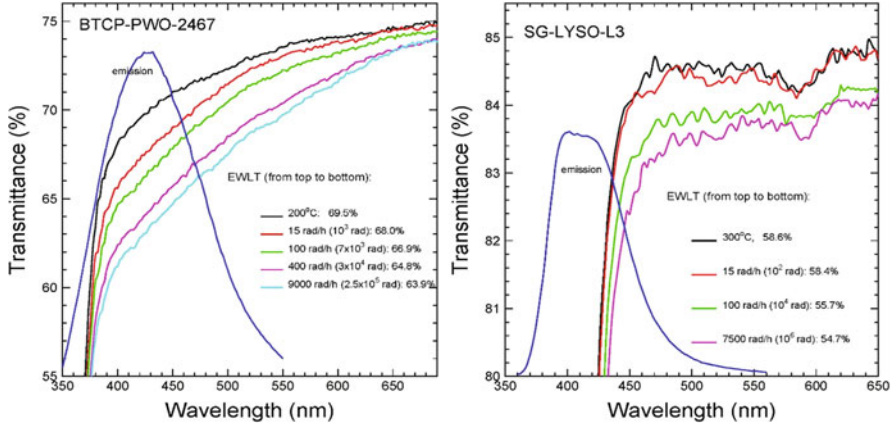
Fig. 4 Degradation on EWLT for a PWO sample (left) and an LYSO sample (right)

observed for BaF_2 as discussed later in section "Dose Rate Dependence and Color Center Kinetics."

It is also interesting to note that the radiation-induced absorption is much smaller in LSO and LYSO than that in other crystals. Figure 4 shows an expanded view of the longitudinal transmittance spectra measured before and after several steps of γ-ray irradiations for a PWO (left) and an LYSO (right) sample. Also shown in the figures is the corresponding photo-luminescence spectra (blue) and the numerical values of the emission weighted longitudinal transmittance (EWLT), which is defined as:

$$EWLT = \frac{\int LT(\lambda) \, Em(\lambda) \, d\lambda}{\int Em(\lambda) \, d\lambda} \tag{1}$$

The EWLT value represents crystal's transparency more accurate than the transmittance at the emission peak, so is widely used in radiation damage studies. This is particularly true for LSO and LYSO, which have a nonnegligible self-absorption since a part of their emission spectra is not within the transparent region of the crystal (Chen et al. 2005).

Recovery of Radiation-Induced Absorption

Depending on color-center depth, the radiation-induced absorption may recover spontaneously at the application temperature. Figure 5 shows typical recovery behavior of the longitudinal optical transmittance at 440 nm and 420 nm, respectively, measured up to 4,000 and 500 h after γ-ray irradiations for two PWO (left) and four LSO and LYSO (right) samples. Three recovery time constants were determined by an exponential fit for PWO samples. While the short time constant
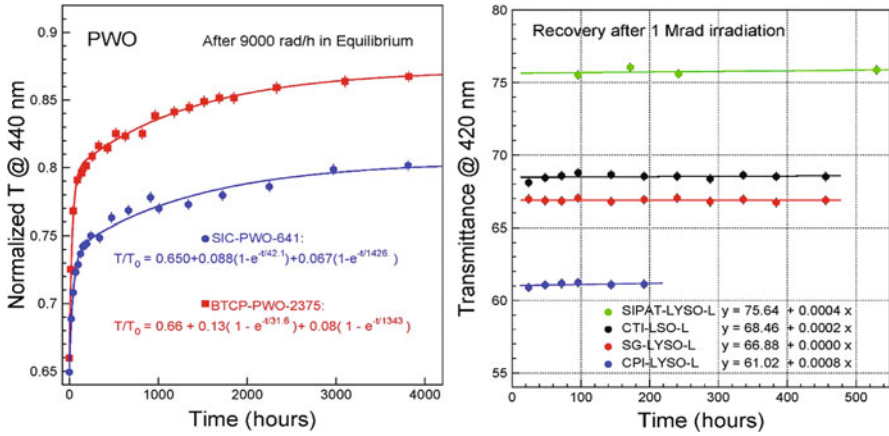
Fig. 5 Recovery of γ-ray-induced transmittance damage is shown as a function of time after irradiation for two PWO samples (left) and four LSO/LYSO samples (right)

is of a few tens of hours, the medium time constant is at a few thousands hours, and the third time constant is much longer, which may be considered as no recovery for the time scale of these measurements. It is also interesting to note that the LSO and LYSO samples show very slow recovery speed, consisting with no recovery. Similarly, the radiation-induced absorption in BaF_2 (Zhu 1994) and CsI:Tl (Zhu et al. 1996a) does not recover as well at room temperature. The radiation damage in LYSO, BaF_2, and CsI crystals thus is not dose rate dependent. On the other hand, the radiation damage in BGO and PWO are dose rate dependent.

In addition to the spontaneous recovery at the application temperature, the radiation damage level may also be reduced by heating crystals to a high temperature (thermal annealing) or injecting light of various wavelength to the crystal (optical bleaching). It is known that γ-ray-induced damage can be completely removed by thermal annealing at 200 °C for BaF_2 (Zhu 1994), BGO (Zhu et al. 1991), and PWO (Zhu et al. 1996b), or 300 °C for LSO and LYSO (Chen et al. 2005). Optical bleaching was also found effective for BaF_2 (Zhu 1994), BGO (Zhu et al. 1991), and PWO (Zhu et al. 1996b). On the other hand, the γ-ray-induced absorption in CsI:Tl can neither be annealed thermally or bleached optically (Zhu et al. 1996a). Optical bleaching may be used to reduce color center density in crystals in situ. Such an approach has been extensively studied for BaF_2 (Ma and Zhu 1993b) and PWO (Zhu et al. 1996b; Yin et al. 1997).

Radiation-Induced Color Centers

Crystal's longitudinal transmittance data can be used to calculate crystal's light attenuation length as a function of wavelength (Ma and Zhu 1993a):

$LAL\left(\lambda\right)$

$$= \frac{l}{\ln\left\{\left[T\left(\lambda\right)\left(1-T_s\left(\lambda\right)\right)^2\right]/\left[\sqrt{4T_s^4\left(\lambda\right)+T^2\left(\lambda\right)\left(1-T_s^2\left(\lambda\right)\right)^2}-2T_s^2\left(\lambda\right)\right]\right\}} \tag{2}$$

where T(λ) is the longitudinal transmittance measured along crystal length l, and $T_s\left(\lambda\right)$ is the theoretical transmittance assuming multiple bouncings between two crystal ends and without internal absorption:

$$T_s\left(\lambda\right) = \left(1-R\left(\lambda\right)\right)^2 + R^2\left(\lambda\right)\left(1-R\left(\lambda\right)\right)^2 + \cdots = \left(1-R\left(\lambda\right)\right)/\left(1+R\left(\lambda\right)\right) \tag{3}$$

and

$$R\left(\lambda\right) = \frac{\left(n_{\text{crystal}}\left(\lambda\right)-n_{\text{air}}\left(\lambda\right)\right)^2}{\left(n_{\text{crystal}}\left(\lambda\right)+n_{\text{air}}\left(\lambda\right)\right)^2} \tag{4}$$

where $n_{\text{crystal}}\left(\lambda\right)$ and $n_{\text{air}}\left(\lambda\right)$ are the refractive indices for crystal and air, respectively.

Radiation-induced absorption coefficient RIAC (λ), or color center density D (λ),and the emission weighted radiation-induced absorption coefficient (EWRIAC) can be calculated as (Ma and Zhu 1993b):

$$RIAC\left(\lambda\right)\ or\ D\left(\lambda\right) = 1/LAL_{\text{after}}\left(\lambda\right) - 1/LAL_{\text{before}}\left(\lambda\right) \tag{5}$$

$$EWRIAC = \frac{\int RIAC\left(\lambda\right)Em\left(\lambda\right)d\lambda}{\int Em\left(\lambda\right)d\lambda} \tag{6}$$

where $LAL_{\text{after}}\left(\lambda\right)$ and $LAL_{\text{before}}\left(\lambda\right)$ are the light attenuation length after and before irradiation, respectively, and $Em(\lambda)$ is the emission spectrum.

The above equations are accurate presentations for crystal's transparency and radiation-induced absorption coefficient. They are light path length independent, so can be used to represent radiation damage level. A simplified representation for $RIAC(\lambda)$ is:

$$RIAC\left(\lambda\right) = \frac{1}{l}\ln\frac{T_0\left(\lambda\right)}{T\left(\lambda\right)} \tag{7}$$

where T0(λ) is the transmittance along crystal length l measured before irradiation and T(λ) is the transmittance measured after irradiation. This equation does not
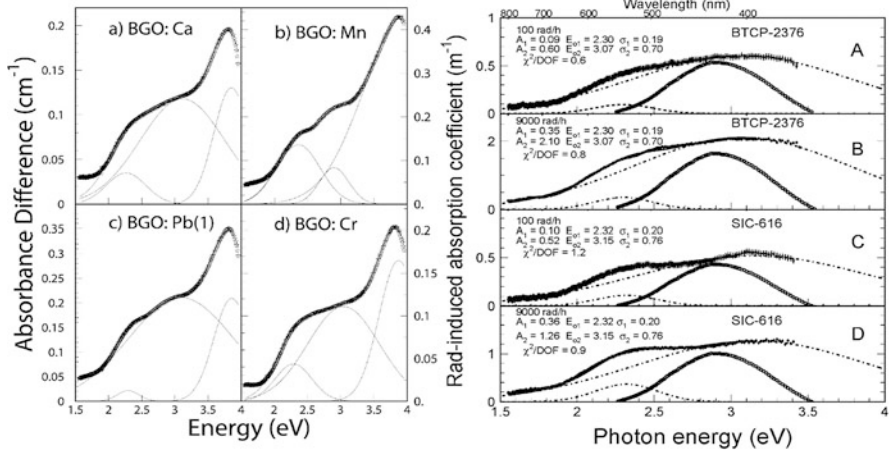
Fig. 6 Radiation-induced absorption coefficient spectra (data points with error bars) are shown as a function of the photon energy for four doped BGO samples (Left) and two PWO samples (Right)

take into account multiple bounces between two end surfaces of the crystal, so is an approximation of the eq. 5 above (Ma and Zhu 1993a).

Spectrum of radiation-induced absorption coefficient can also be presented as a function of the photon energy, and be further decomposed to a sum of several color centers with Gaussian energy distributions (Zhu et al. 1991):

$$RIAC\,(\lambda) = \sum_{i=1}^{n} A_i e^{-\frac{(E(\lambda)-E_i)^2}{2\sigma_i^2}} \tag{8}$$

where E_i, σ_i, and D_i denote the energy, width, and amplitude of the color center i, respectively, and $E(\lambda)$ is the photon energy.

Figure 6 shows the radiation-induced absorption coefficient as a function of the photon energy for four BGO samples doped with Ca, Mn, Pb, and Cr (left) and two PWO samples in the equilibrium under γ-ray irradiation with dose rates of 100 rad/h and 9,000 rad/h (right). It is interesting to note that although the overall shapes of radiation-induced absorption coefficients are different, the color centers are located at the same energy and with the same width for both crystals. While there are three color centers peaked at 2.3 eV, 3.0 eV, and 3.8 eV for the BGO samples, the PWO samples show two color centers peaked at 2.3 eV and 3.1 eV. This observation hints that the color centers in these oxide crystals are caused by crystal structure–related defects, such as oxygen vacancies, not particular impurities. Readers are referred to the corresponding references (Zhu et al. 1991, 1996b) for more discussions about the color centers in these crystals .

Dose Rate Dependence and Color Center Kinetics

Because of the balance between two dynamic processes: a color center creation process (irradiation) and a color center annihilation process (room temperature recovery), radiation damage in inorganic scintillators is usually dose rate dependent. Assuming that the annihilation speed of the color center i is proportional to a constant a_i and its creation speed is proportional to a constant b_i and the dose rate (R), the differential change of color center density when both processes coexist can be expressed as (Ma and Zhu 1993b):

$$dD\left(\lambda\right) = \sum_{i=1}^{n}\left\{-a_i\,D_i\left(\lambda\right)dt + \left(D_i^{all}\left(\lambda\right) - D_i\left(\lambda\right)\right)b_i\,Rdt\right\} \qquad (9)$$

where $D_i\left(\lambda\right)$ is the density of the color center i in the crystal, and the summation goes through all the centers. The solution of Eq. 9 is

$$D\left(\lambda\right) = \sum_{i=1}^{n}\left\{\frac{b_i\,RD_i^{\text{all}}\left(\lambda\right)}{a_i + b_i\,R}\left[1 - e^{-(a_i + b_i\,R)t}\right] + D_i^0\left(\lambda\right)e^{-(a_i + b_i\,R)t}\right\} \qquad (10)$$

where $D_i^{\text{all}}\left(\lambda\right)$ is the total density of the trap related to the color center i and the $D_i^0\left(\lambda\right)$ is its initial value. The color center density in the equilibrium $D_{\text{eq}}\left(\lambda\right)$ depends on the dose rate R:

$$D_{\text{eq}}\left(\lambda\right) = \sum_{i=1}^{n}\frac{b_i\,RD_i^{\text{all}}\left(\lambda\right)}{a_i + b_i\,R} \qquad (11)$$

Following these equations, crystal's optical transmittance, and thus crystal's light output, decreases when the crystal is exposed to a radiation under a dose rate R, and would reach an equilibrium. At the equilibrium, the speed of the color center formation (damage) equals to the speed of the color center annihilation (recovery), so that the color center density, or radiation-induced absorption, does not change unless the dose rate (R) or temperature (a_i) changes. Applying a bleaching light introduces an additional color center annihilation process (a_i), thus changes the color center density at the equilibrium as well. More detailed discussions on the behavior of the color center densities with a bleaching light applied can befound in (Ma and Zhu 1993b).

Equation 11 also indicates that the radiation damage level does not depend on the dose rate if the recovery speed (a_i) is small, which is the characteristics of the radiation damage caused by deep color centers. For crystals with no dose rate dependence, an accelerated irradiation with a high dose rate would lead to the same effect as a slow irradiation with a low dose rate provided that the total integrated dose is the same. This is clearly shown in the transmittance data of a BaF$_2$ crystal in the top right plot of Fig. 3.

Light Output Degradation

Crystal's light output is a convolution of crystal's emission, light propagation inside the crystal, and the quantum efficiency (QE) of the photo-detector. All these are wavelength-dependent. Since crystal emission and photo-detector QE are usually not affected by radiation, the degradation of crystal's light output is correlated to the degradations of crystal's transparency, i.e., the radiation-induced absorption. A light monitoring system, which measures variations of crystal's transparency, thus provides necessary information for calibration of crystal's light output in situ under radiation. It is also clear that degradation of crystal's light output is light path length dependent. Crystals of small size thus suffer less radiation damage than crystals of large size.

In HEP experiments, radiation in situ is expected from ionization dose, charged hadrons, and neutrons. During the LHC Run-I, significant light output losses were observed by the CMS light monitoring system for PWO crystals (T. Dimova on behalf of the CMS Collaboration 2017). With a 5×10^{34} cm^{-2} s^{-1} luminosity and a 3,000 fb^{-1} integrated luminosity (▶ Particle Identification), the HL-LHC will present a radiation environment, where up to 130 Mrad ionization dose, 3×10^{14} charged hadrons/cm^2, and 5×10^{15} fast neutron/cm^2 are expected (Bilki 2015). In this section, light output degradation induced by ionization dose, protons, and neutrons with an integrated dose up to 340 Mrad, a proton fluence up to 3.0×10^{15} p/cm^2, and a fast neutron fluence up to 3.0×10^{15} n/cm^2, respectively, is presented for various crystals, thus putting an emphasis on LYSO, BaF$_2$, and PWO crystals.

Ionization Dose–Induced Radiation Damage

Ionization dose–induced radiation damage was investigated at the Total Ionization Dose (TID) facility of Jet Propulsion Laboratory. Figure 7 shows normalized EWLT (top) and light output (LO, bottom) as a function of the integrated dose for six LYSO/LSO/LFS crystals (left) and three BaF$_2$ crystals from different vendors, where the fast scintillation component peaked at 220 nm with sub-ns decay time is shown for BaF$_2$. The losses of EWLT and light output are at a level about 40–60% for both LYSO and BaF$_2$ crystals after 100 Mrad, showing excellent radiation hardness of these crystals. It is also interesting to note that while the light output of BaF$_2$ degrades below 10 krad, it is more or less stabilized after that, which is consistent with the transmittance data shown in Fig. 3 (Zhu 1994).

Figure 8 shows the RIAC values at the emission peak (left) and the normalized light output (right) as a function of the integrated dose for various crystal samples of large size (Yang et al. 2016a). We note that beyond 1 Mrad LYSO, BaF$_2$ and BGO crystals show significantly better radiation hardness than CeF$_3$, CsI, and PWO. In terms of light output loss, LYSO is the best among all crystal scintillators. The best sample of this type maintains 75% and 60% light output, respectively, after
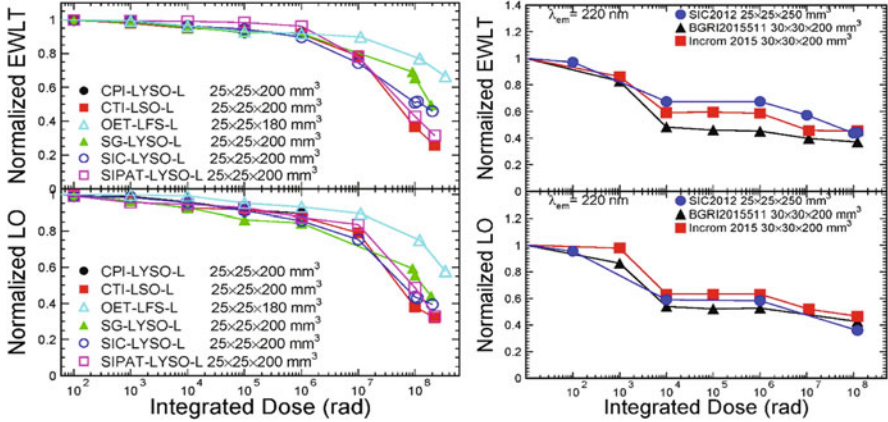
Fig. 7 Normalized EWLT (top) and light output(bottom) are shown as a function of the ionization dose up to 340 and 120 Mrad, respectively, for six LYSO/LSO/LFS crystals (left) and three BaF_2 crystals (right) from different vendors
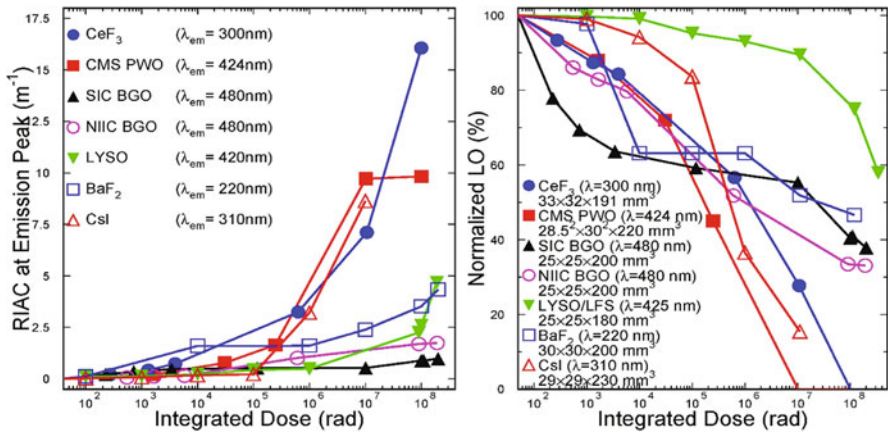

Fig. 8 The RIAC values at the emission peak (Left) and the normalized light output (Right) are shown as a function of integrated dose for various crystal scintillators

120 and 340 Mrad. On the other hand, BaF_2 and BGO crystals also maintain 45% and 35% light output, respectively, after 120 and 200 Mrad, so may be considered as cost-effective alternatives for future HEP experiments in a severe radiation environment. Undoped CsI shows good radiation hardness below 100 krad, so is a cost-effective choice for future HEP experiments in a modest radiation environment (▶ Gamma-Ray Detectors).
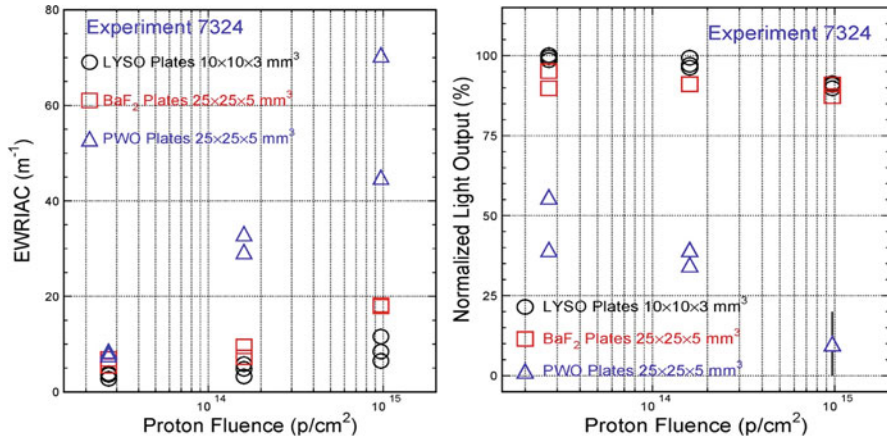
Fig. 9 The EWRIAC values (left) and the normalized light output (right) are shown as a function of the integrated 800 MeV proton fluence for LYSO, BaF$_2$, and PWO crystal plates

Proton-Induced Radiation Damage

Following early studies (Huhtinen et al. 2005; Dissertori et al. 2010, 2014; Yang et al. 2016b; Auffray et al. 2012, 2013; Dormenev et al. 2014; Lecomte et al. 2006), proton-induced radiation damage was investigated at the Weapons Neutron Research facility of Los Alamos Neutron Science Center (WNR of LANSCE) (Hu et al. 2018a). A total of 21 samples (six each for BaF$_2$ and PWO of $25 \times 25 \times 5$ mm^3 and nine LYSO of $10 \times 10 \times 3$ mm^3) were irradiated by 800 MeV protons in three batches to reach 2.7×10^{13}, 1.6×10^{14} and 9.7×10^{14} p/cm^2. Samples were measured 183 days after irradiation.

Figure 9 shows their EWRIAC values (left) and the normalized light output (right) as a function of the proton fluence. The EWRIAC values are 7, 18, and 71 m^{-1}, respectively, for LYSO, BaF$_2$, and PWO after a proton fluence of 9.7×10^{14} p/cm^2. The light output losses are 10% and 13%, respectively, for the LYSO and BaF$_2$, indicating excellent radiation hardness of LYSO and BaF$_2$ crystals against charged hadrons. The light output of PWO samples after proton fluence of 9.7×10^{14} p/cm^2 is too low to be experimentally determined.

Neutron-Induced Radiation Damage

Early works did not find clean evidence on neutron-induced damage in scintillating crystals (Chipaux et al. 2005; Zhang et al. 2009). While the investigation presented in (Zhang et al. 2009) was carried out for a fast neutron fluence up to 6×10^8 n/cm^2, that in (Chipaux et al. 2005) was carried out for PWO crystals up to a fast neutron fluence of 10^{19} n/cm^2. Following these studies, neutron-induced radiation damage was investigated at WNR of LANSCE by using a combination of particles,
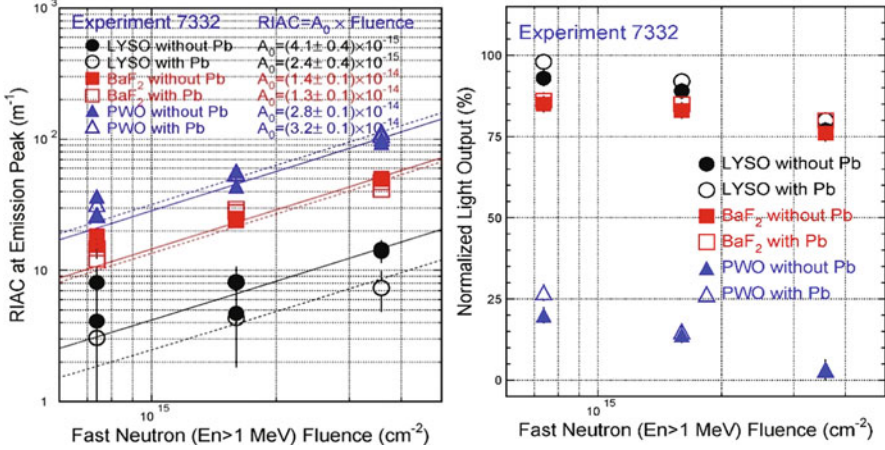
Fig. 10 The RIAC values at the emission peak (left) and the normalized light output (right) are shown as a function of the integrated fast neutron fluence for LYSO, BaF$_2$, and PWO crystal plates

including neutrons, protons, and γ-rays with a fast neutron (>1 MeV) fluence up to 3.6×10^{15} n/cm^2, a proton fluence up to 1×10^{13} p/cm^2, and 5 Mrad of ionization dose (Hu et al. 2018b). A total of 36 samples, 12 each for BaF$_2$, LYSO, and PWO of $10 \times 10 \times 5$ mm^3, were irradiated in three batches for 21.2, 46.3, and 120 days to reach fast neutron fluences of 7.4×10^{14}, 1.6×10^{15}, and 3.6×10^{15} n/cm^2, respectively. In this experiment a half of the samples were shielded with 5 mm lead to reduce the ionization dose background. Samples were measured 189, 164, and 90 days after the irradiation.

Figure 10 shows their RIAC values at the emission peak (left) and the normalized light output (right) as a function of the fast neutron (>1 MeV) fluence. While the average RIAC values of two samples each after a fast neutron fluence of 3.6×10^{15} n/cm^2 are 14.1, 49.8, and 97.1 m^{-1}, respectively, for LYSO, BaF$_2$, and PWO without 5 mm Pb shielding, the corresponding values are 7.3, 44.2, and 110.5 m^{-1} with Pb shielding. The corresponding light output losses after 3.6×10^{15} n/cm^2 are 23% and 24%, respectively, for LYSO and BaF$_2$ crystals without Pb shielding, and 20% and 20% with Pb shielding. In both cases, the light output of PWO samples after a fast neutron fluence of 3.6×10^{15} n/cm^2 is too low to be experimentally determined. The data point for the PWO crystals in the group 3 thus indicates an upper limit. It is clear that LYSO and crystals are more radiation hard than PWO under neutron irradiations.

It is interesting to note that the damage observed here is more than a factor of ten larger than the damage expected by the 5 Mrad ionization dose along with 1×10^{13} p/cm^2 proton fluence. These data thus show a clear evidence of neutron-induced radiation damage in these scintillating crystals. Additional investigation with an effective Pb shielding for ionization dose background would be useful to clarify the nature of neutron-induced damage, compared to ionization dose and/or charged hadrons–induced damages.

Light Response Uniformity

An adequate light response uniformity along crystal length is a key for maintaining excellent energy resolution promised by a total absorption crystal calorimeter. Light output along a long crystal *LO (x)* may be parameterized as a linear function

$$\frac{LO(x)}{LO_{\text{mid}}} = 1 + \delta\,(x/x_{\text{mid}} - 1) \tag{12}$$

where LO_{mid} represents the light output measured at the middle point of the crystal, δ represents the deviation from a flat response, and x is the distance from one end of the crystal. An alternative measure of light response uniformity is the rms values of the light out values measured along the crystal length. Commercially available crystals of a rectangular shape have a flat light response uniformity, but may also be the photo-detector coupling end dependent. A common practice is to choose the coupling end which provides a better light response uniformity.

Figure 11 shows the light response uniformity for a PWO sample (left) and an LYSO sample (right) after several steps of γ-ray irradiation. The γ-ray irradiation was carried out step by step under a fixed dose rate to reach an integrated dose in each step. It is clear that the δ values were not changed for both crystals, indicating that the energy resolution would not be compromised after the γ-ray irradiation. This is due to the fact that the degraded light attenuation length is long enough to maintain the light response uniformity as predicted by ray-tracing simulations (Zhu 1998).
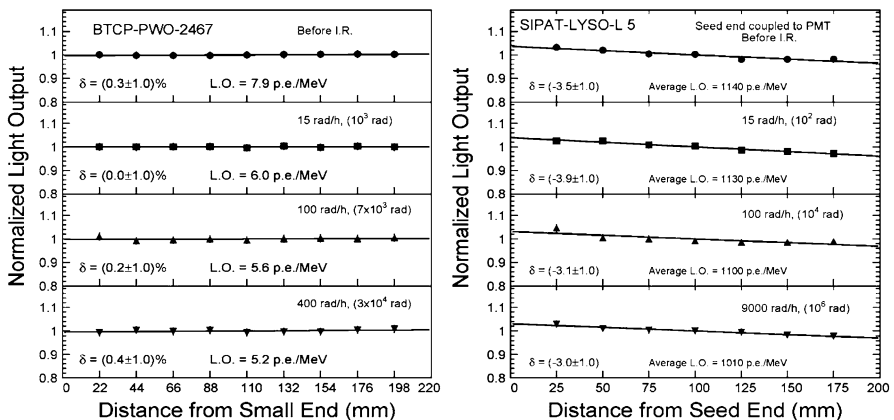

Fig. 11 Light output is shown as a function of the distance to the end coupled to PMT for a PWO samples (left) and an LYSO sample (right) after several steps of γ-ray irradiations

Damage Mechanism in Alkali Halide Crystals and CsI:Tl Development

Material analysis is important for investigations on the radiation damage mechanism. Glow Discharge Mass Spectroscopy (GDMS) analysis was used to identify trace impurities harmful to radiation hardness for a batch of CsI:Tl crystals. Samples were taken 3–5 mm below the surface of the crystal to avoid surface contamination. A survey of 76 elements, including all of the lanthanides, indicates that there are no obvious correlations between the detected trace impurities and the crystal's susceptibility to the radiation damage. This hints an important role of the oxygen contamination which cannot be determined by GDMS analysis.

Oxygen contamination is known to cause radiation damage in the alkali halide scintillators. In BaF$_2$ (Zhu 1994), for example, hydroxyl (OH^-) may be introduced into crystal through a hydrolysis process, and later decomposed to interstitial and substitutional centers by radiation through a radiolysis process. Equation 13 shows a scenario of this process:

$$OH^- \rightarrow H_i^0 + O_s^- \ or \ H_s^- + O_i^0 \tag{13}$$
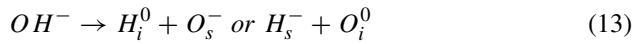
where the subscript i and s refer to the interstitial and substitutional centers, respectively. Both the O_s^- center and the U center (H_s^-) were identified (Zhu 1994).

Following the BaF$_2$ experience, significant improvement of the radiation hardness was achieved for CsI(Tl) crystals by using a scavenger to remove oxygen contamination (Zhu et al. 1996a). Figure 12 (left) shows normalized light output as a function of the integrated dose for a group of CsI(Tl) samples, and compared to the *BaBar* radiation hardness specification (solid lines) (Zhu 1998). While the late samples SIC-5, 6, 7, and 8 satisfy the *BaBar* specification, early samples SIC-2 and 4 do not.

This improvement of CsI(Tl) quality was achieved following an understanding that the radiation damage in the halide crystals is caused by the oxygen orhydroxyl contamination. Various material analysis was carried out to quantitatively identify the oxygen contamination in the CsI(Tl) samples. Gas fusion (LECO), for example, was found not sensitive enough to identify the oxygen contamination. The identification of oxygen contamination was finally achieved by using the secondary ionization mass spectroscopy (SIMS) analysis. A Csion beam of 6 keV and 50 nA was used to bombard the CsI(Tl) samples. All samples were freshly cleaved prior being loaded into the UHV chamber. An area of $0.15 \times 0.15 \text{ mm}^2$ on the cleaved surface was analyzed. To further avoid the surface contamination, the starting point of the analysis is at about 10 µm deep inside the fresh cleaved surface. Figure 12 (right) shows the depth profile of the oxygen contamination for two radiation soft samples (SIC-T1 and SIC-2) and two radiation hard samples (SIC-T3 and Khar'kov). Crystals with poor radiation resistance have oxygen contamination of 10^{18}atoms/cm^3 or 5.7 PPMW, which is 5 times higher than the background count (2×10^{17} atoms/cm^3, or 1.4 PPMW).
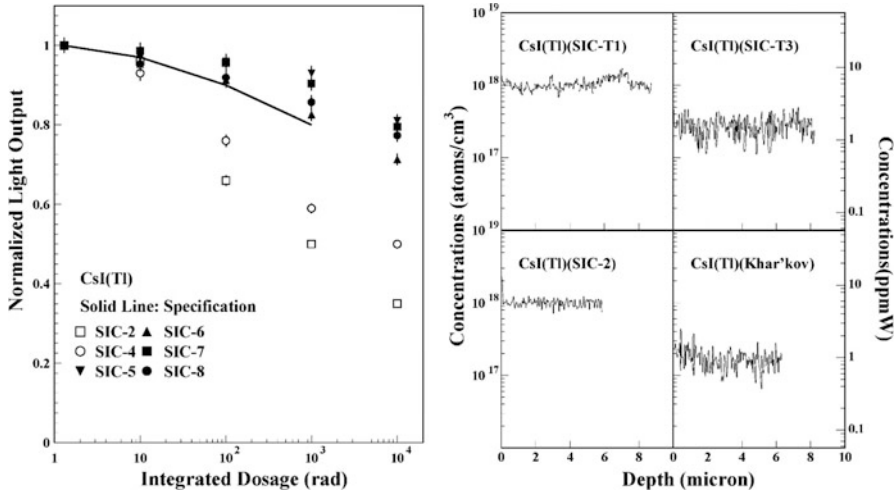
Fig. 12 Left: The progress of the CsI(Tl) radiation hardness is shown for CsI(Tl) samples from SIC together with the *BaBar* radiation-hardness specification. Right: The depth profile of the oxygen contamination is shown for two rad-soft CsI(Tl) samples (SIC-T1 and SIC-2) and two rad-hard samples (SIC-T3 and Khar'kov)

Damage Mechanism in Oxide Crystals and PWO Development

Similarly, GDMS analysis was used for BGO and PWO crystals, and was found no particular correlation with crystal's radiation hardness. This hints an important role of the structure-related defects in the crystal, which cannot be determined by the GDMS analysis. Crystal structure defects, such as oxygen vacancies, are known to cause radiation damage in oxide scintillators. In BGO, for example, three common radiation-induced absorption bands at 2.3 eV, 3.0 eV, and 3.8 eV were found in a series of 24 doped samples (Zhu et al. 1991) as shown in the left plot of Fig. 6. Observations in the PWO crystals are similar with two color centers peaked at 2.3 eV and 3.1 eV as shown in the right plot of Fig. 6.

Following these observations, effort was made to reduce oxygen vacancies in PWO crystals. An oxygen compensation approach, which was carried out by a postgrowth thermal annealing in an oxygen-rich atmosphere, was found effective in improving PWO's radiation hardness for samples up to 10 cm long (Zhu et al. 1996b). This approach, however, is less effective for longer (25 cm) crystals because of the variation of the oxygen vacancies along the crystal.

In practice, yttrium doping, which provides a local charge balance for oxygen vacancies to prevent the color center formation, was found effective for PWO (Zhu et al. 1996b). Figure 13 shows the normalized light output as a function of time for three PWO samples under the γ-ray irradiations with a dose rate of 15 rad/h. PWO samples produced after 2002 with yttrium doping is much more radiation hard than the early samples.
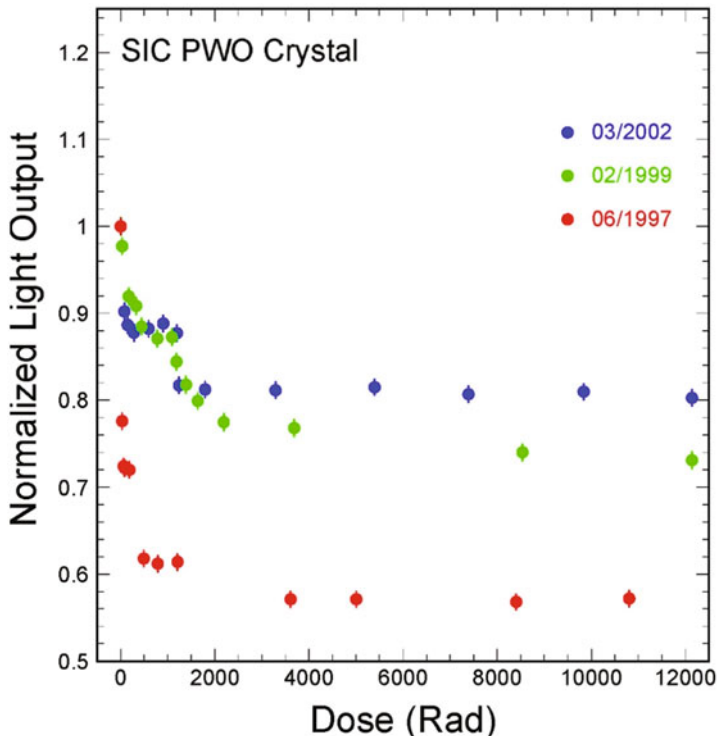
Fig. 13 The progress of PWO radiation hardness is shown for PWO samples from SIC

This improvement of PWO quality was achieved following an assumption that the radiation damage in the oxide crystals is caused by the oxygen vacancies. Various material analysis was carried to quantitatively identify the stoichiometry deviation and the oxygen vacancies in the PWO samples. Particle-induced X-ray emission (PIXE) and quantitative wavelength dispersive electron micro-probe analysis (EMPA) were tried. PWO crystals with poor radiation hardness were found as having a nonstoichiometric W/Pb ratio. Both PIXE and EMPA, however, do not provide quantitative oxygen analysis. X-ray photoelectron spectroscopy (XPS) was found to be very difficult because of the systematic uncertainty in oxygen analysis. Electron paramagnetic resonance (ESR) and electron-nuclear double resonance (ENDOR) were tried to find unpaired electrons, but were also found to be difficult to reach a quantitative conclusion.

The final identification of the oxygen vacancies is achieved by using the transmission electron microscopy (TEM) coupled to energy dispersion spectrometry (EDS) with a localized stoichiometry analysis. A TOPCON-002B scope was first used at 200 kV and 10 μA. The PWO samples were made to powders of an average grain size of a few μm, and then placed on a sustaining membrane. With a spatial resolution of 2 Å, the lattice structure of the PWO samples was clearly visible.
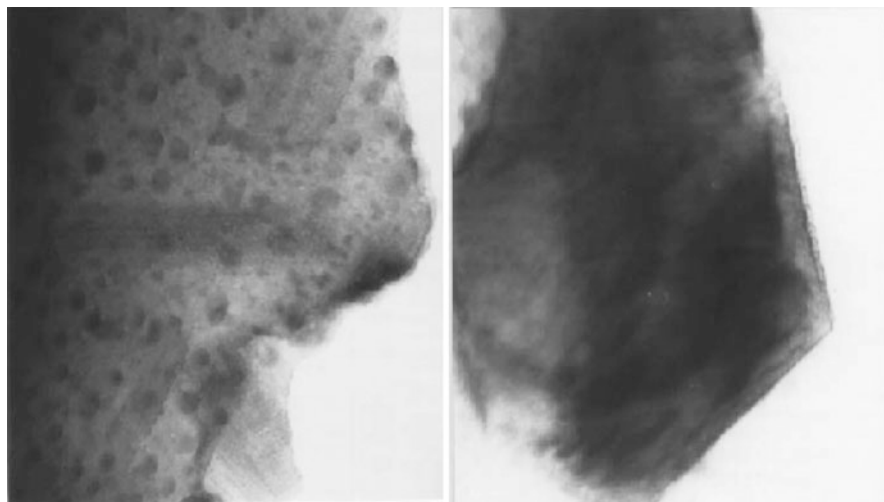
Fig. 14 TEM pictures of a PWO crystal of poor radiation hardness (left), showing clearly the black spots of ϕ5–10 nm related to oxygen vacancies, as compared to that of a good one (right)

Table 3 Atomic fraction (%) of O, W, and Pb in PWO samples measured by TEM/EDS (Yin et al. 1997)

As grown sample				
Element	Black spot	Peripheral	Matrix$_1$	Matrix$_2$
O	1.5	15.8	60.8	63.2
W	50.8	44.3	19.6	18.4
Pb	47.7	39.9	19.6	18.4
The same sample after oxygen compensation				
Element	Point$_1$	Point$_2$	Point$_3$	Point$_4$
O	59.0	66.4	57.4	66.7
W	21.0	16.5	21.3	16.8
Pb	20.0	17.1	21.3	16.5

Figure 14 shows TEM pictures taken for a sample with poor (left) and good (right) radiation hardness. Black spots of a diameter of 5–10 nm were clearly observed in the sample with poor radiation hardness, but not in the sample with good radiation hardness. A TEM/EDS stoichiometry analysis was carried out by using a JEOL JEM-2010 scope and a Link ISISEDS. The fine spatial resolution of this system allows a localized stoichiometry analysis in an area down to 0.5 nm diameter. Table 3 lists result atomic fractions (%) in for areas inside and surrounding the black spots as well as far away from the black spots (Matrix) (Yin et al. 1997). The systematic uncertainty of this analysis is about 15%.

A clear deviation from the atomic stoichiometry of O:W:Pb = 66:17:17 was observed for samples taken inside these black spots, revealing a severe oxygen deficit. In the peripheral area, the oxygen deficit was less, but still significant. There was no oxygen deficit observed in the area far away from the black spots.

As a comparison, the same sample after a thermal annealing in an oxygen-rich atmosphere was re-analyzed. No black spot was found. The result of the analysis is also listed in Table 3. In all randomly selected points, no stoichiometry deviation was observed. This analysis thus clearly identified oxygen vacancies in PWO samples of poor radiation hardness .

Conclusion

Inorganic scintillators suffer from radiation damage with the following possible consequences: (1) scintillation mechanism damage, (2) radiation-induced phosphorescence, and (3) radiation-induced absorption. No experimental evidence has been observed for scintillation mechanism damage in any crystals studied so far. All crystals show radiation-induced phosphorescence and absorption. Radiation-induced phosphorescence increases dark current in photo-detector, and thus the readout noise. This leads to energy equivalent noise, which is low for crystals with high light yield. The predominant radiation damage effect in the crystal scintillators is the radiation-induced absorption, or color center formation. Radiation-induced absorption may recover spontaneously at the application temperature, and leads to a dose rate dependence. Thermal annealing and optical bleaching are effective for shallow color centers, but may not for deep color centers.

While radiation damage induced by ionization dose is well understood, hadron-specific radiation damage in inorganic scintillators is under investigation, which is very important for future high energy physics experiments at the energy frontier. Recent data obtained at LANSCE show that LYSO and BaF_2 crystals are more radiation hard than PWO under proton and fast neutron fluences up to a few $\times$ $10^{15}/cm^2$. Additional investigation is needed to fully understand hadron-specific radiation damage.

Radiation damage in alkali halide crystals is understood to be caused by the oxygen and/or hydroxyl contamination as demonstrated by a SIMS analysis. Radiation hardness of the mass produced CsI(Tl) crystals is improved by using a scavenger to remove oxygen contamination. Radiation damage in oxide crystals is found to be caused by stoichiometry-related defects, e.g., oxygen vacancies, as demonstrated by a localized stoichiometry analysis with TEM/EDS. Yttrium doping improves radiation hardness of the mass produced PWO crystals.

Cross-References

▶ Calorimeters
▶ Gamma-Ray Detectors
▶ Particle Identification
▶ Scintillators and Scintillation Detectors

References

Auffray E, Korjik M, Singovski A (2012) Experimental study of lead tungstate scintillator proton-induced damage and recovery. IEEE Trans Nucl Sci 59:2219–2223

Auffray E, Barysevich A, Fedorov A, Korjik M, Koschan M, Lucchini M, Mechinski V, Melcher CL, Voitovich A (2013) Radiation damage of LSO crystals under γ -and 24 GeV protons irradiation. Nucl Instrum Meth A721:76–82

Batarin VA, Butkler J, Chen TY, Davidenko AM, Derevschikov AA, Goncharenko YM et al (2003) Study of radiation damage in lead tungstate crystals using intense high-energy beams. Nucl Instrum Meth A512:488–505, 530:286–292 (2004) and 540:131–139 (2005)

Bilki B (2015) CMS forward calorimeters phase II upgrade. J Phys Conf Ser 587:012014

Chen JM, Mao RH, Zhang LY, Zhu R-Y (2005) Large size LYSO crystals for future high energy physics experiments. IEEE Trans Nucl Sci 52:2133–2140. and IEEE Trans Nucl Sci 54:718–724 (2007)

Chipaux R, Korzhik MV, Borisevich A, Lecoq P, Dujardin C (2005) Behaviour of PWO scintillators after high fluence neutron irradiation. In: Getkin A, Grinyoveds B (eds) Proceedings of the 8th international conference on inorganic scintillators, SCINT2005, Alushta, Crimea, 19–23 September 2005, pp 369–371

Cooke DW, McClellan KJ, Bennett BL, Roper JM, Whittaker MT, Muenchausen RE (2000) Crystal growth and optical characterization of cerium-doped $Lu_{1.8}Y_{0.2}SiO_5$. J Appl Phys 88:7360–7362

Dissertori G, Lecomte P, Luckey D, Nessi-Tedaldi F, Pauss F, Otto T, Roesler S, Urscheler C (2010) A study of high-energy proton induced damage in cerium fluoride in comparison with measurements in lead tungstate calorimeter crystals. Nucl Instrum Meth A622:41–48

Dissertori G, Luckey D, Nessi-Tedaldi F, Pauss F, Quittnat M, Wallny R, Glaser M (2014) Results on damage induced by high-energy protons in LYSO calorimeter crystals. Nucl Instrum Meth A745:1–6

Dormenev V, Korjik M, Kuske T, Mechinski V, Novotny RW (2014) Comparison of radiation damage effects in PWO crystals under 150 MeV and 24 GeV high fluence proton irradiation. IEEE Trans Nucl Sci 61:501–506

Gratta G, Newman H, Zhu R-Y (1994) Crystal calorimeters in particle physics. Annu Rev Nucl Part Sci 44:453–500

Hu C, Yang F, Zhang L, Zhu R-Y, Kapustinsky J, Nelson R, Wang Z (2018a) Proton-induced radiation damage in BaF_2, LYSO and PWO crystal scintillators. IEEE Trans Nucl Sci 65:1018–1024

Hu C, Yang F, Zhang L, Zhu R-Y, Kapustinsky J, Mocko M, Nelson R, Wang Z (2018b) Neutron-induced radiation damage in BaF_2, LYSO/LFS and PWO crystals. Presented at Calor2018 conference, will appear in Journal of Physics: Conference Series, Oregon. IEEE Trans Nucl Sci 67:1086–1092

Huhtinen M, Lecomte R, Lucky D, Nessi-Redaldi F, Pauss F (2005) High-energy Proton Induced Damage in $PbWO_4$ calorimeter crystals. Nucl Instrum Meth A545:63, 564 (2006) 164 and 587 (2008) 266

Kimble T, Chou M, Chai BHT (2002) Scintillation properties of LYSO crystals. In: IEEE NSS conference record, Norfolk, pp 1434–1437

Lecomte P, Luckey D, Nessi-Tedaldi F, Pauss F (2006) Highenergy proton induced damage study of scintillation light output from PbWO4 calorimeter crystals. Nucl Instrum Meth A564: 164–168

Ma DA, Zhu R-Y (1993a) Light attenuation length of barium fluoride crystals. Nucl Instrum Meth A333:422–424

Ma DA, Zhu R-Y (1993b) On optical bleaching of barium fluoride crystals. Nucl Instrum Meth A332:113–120. and Nucl Instrum Meth A356:309–318 (1995)

Mao RH, Zhang LY, Zhu R-Y (2008) Optical and scintillation properties of inorganic scintillators in high energy physics. IEEE Trans Nucl Sci NS-55:2425–2431

Mao RH, Zhang LY, Zhu R-Y (2009a) Gamma ray induced radiation damage in PWO and LSO/LYSO crystals. Paper N32-5 in IEEE NSS 2009 conference record, Orlando

Mao RH, Zhang LY, Zhu R-Y (2009b) Effect of neutron irradiations in various crystal samples of large size for future crystal calorimeter. Paper N32-4 in IEEE NSS 2009 conference record, Orlando

Melcher C, Schweitzer J (1992) Cerium-doped lutetium oxyorthosilicate: a fast efficient new scintillator. IEEE Trans Nucl Sci NS-39:502–505

Semenov PA, Uzunia AV, Davidenko AM, Derevschikov AA, Goncharenko YM, Kachanov VA et al (2007) First Study of Radiation Hardness of Lead Tungstate Crystals at Low Temperature. Nucl Instrum Meth A562:575–580, IEEE Trans Nucl Sci NS-55:1283–1288 (2008) and Paper N32-2 in IEEE NSS 2009 Conference Record (2009)

T. Dimova on behalf of the CMS Collaboration. Monitoring and correcting for response changes in the CMS lead-tungstate electromagnetic calorimeter in LHC run2. Presented at the Instrumentation for Colliding Beam Physics, Novosibirsk, Feb/Mar 2017

Yang F, Zhang L, Zhu R-Y (2016a) Gamma-ray induced radiation damage up to 340 Mrad in various scintillation crystals. IEEE Trans Nucl Sci 63:612–619

Yang F, Zhang L, Zhu R-Y, Kapustinsky J, Nelson R, Wang Z (2016b) Proton induced radiation damage in fast crystal scintillators. Nucl Instrum Meth A824:726–728

Yin ZW, Li PJ, Feng JW (1997) TEM study on lead tungstate crystals. In: Yin Z et al (ed) Proceedings of SCINT97 international conference edition, CAS, Shanghai Branch Press, pp 191–194

Zhang L, Mao R, Zhu R-Y (2009) Effects of neutron irradiations in various crystal samples of large size for future crystal calorimeter. In: 2009 IEEE nuclear science symposium conference record (NSS/MIC), Orlando, pp 2041–2044

Zhu RY (1994) On quality requirements to the barium fluoride crystals. Nucl Instrum Meth A340:442–457

Zhu RY (1997) Precision crystal calorimetry in future high energy colliders. In: IEEE NSS1996 Conference Record, published in IEEE Trans Nucl Sci, Anaheim, NS-44:468–476

Zhu R-Y (1998) Radiation damage in scintillating crystals. Nucl Instrum Meth A413:297–311. And references therein

Zhu RY, Stone H, Newman H, Zhou TQ, Tan HR, He CF (1991) a study on radiation damage in doped BGO crystals. Nucl Instrum Meth A302:69–75

Zhu RY, Ma DA, Wu H (1996a) CsI(Tl) radiation damage and quality improvement. In: Antonelli A et al (ed) Proceedings of the 6th international conference on calorimetry in high energy physics. Frascati Physics Series, Frascati, pp 589–598

Zhu RY, Ma DA, Newman HB, Woody CL, Kierstead JA, Stoll SP, Levy PW (1996b) A study on the properties of lead tungstate crystals. Nucl Instrum Meth A376:319–334, IEEE Trans Nucl Sci 45:688–691 (1998), Nucl Instrum Meth A438:415–420 (1999), Nucl Instrum Meth A480:470–487 (2002) and IEEE Trans Nucl Sci 51:1777–1783 (2004)

Further Reading

Claeys C, Simoen E (2002) Radiation effects in advanced semiconductor materials and devices. Springer

Claude L, Pier-Giorgio R (2016) Principles of radiation interaction in matter and detection. 4th edition, World Scietific

Grupen C, Shwartz B (2008) Particle detectors. Cambridge University Press
Holmes-Siedle A, Adams L (2002) Handbook of radiation effects. Oxford University Press
Iniewski K (2010) Radiation effects in semiconductors. CRC Press
Knoll G (2000) Radiation detection and measurement, 3rd edn. Wiley
Lecoq P, Annekov A, Gektin A, Korzhik M, Pedrini C (2005) Inorganic scintillators for detector
    systems. Springer